The magnetic transitions and dynamics in the multiferroic $Lu_{0.5}Sc_{0.5}FeO_3$

Junjie Yang, Chunruo Duan, John R. D. Copley, Craig M. Brown and Despina Louca

MRS Advances / Volume 1 / Issue 09 / January 2016, pp 565 - 571
DOI: 10.1557/adv.2016.141, Published online: 22 February 2016

MRS Advances © 2016 Materials Research Society
DOI: 10.1557/adv.2016.141

The magnetic transitions and dynamics in the multiferroic $Lu_{0.5}Sc_{0.5}FeO_3$

Junjie Yang[1], Chunruo Duan[1], John R. D. Copley[2], Craig M. Brown[2,3] and Despina Louca[1]
[1]Department of physics, University of Virginia, Charlottesville, VA 22903, U.S.A.
[2]Center for Neutron Research, National Institute of Standards and Technology, Gaithersburg, MD 20899, U.S.A.
[3]Department of Chemical and Biomolecular Engineering, University of Delaware, Newark, DE 19716, U.S.A.

ABSTRACT

In spite of its frustrated lattice, the multiferroic $Lu_{0.5}Sc_{0.5}FeO_3$ exhibits two consecutive magnetic transitions at $T_{N1} \approx 175$ K and $T_{N2} \approx 70$ K determined from neutron diffraction. In the ordered state, magnetic fluctuations are present, most likely arising from the in-plane frustrated interaction of the Fe hexagonal lattice. Furthermore, a crossover of the magnetic intensity is observed from elastic to inelastic upon warming, indicating that magnetic fluctuations persist well above T_{N1}, a common feature in hexagonal multiferroics.

INTRODUCTION

Multiferroics of the kind that exhibit successive ferroelectric and magnetic orders have captivated the research community in large part due to their unique properties. Among the various multiferroic materials, one of the earliest examples is that of the hexagonal RMnO$_3$ family (R is a rare earth ion with small radius such as Y, Lu, Ho, and Yb) with space group $P6_3cm$.[1-6] Recently, the isostructural RFeO$_3$ (R=Y, Yb and Lu) family has been made with an antiferromagnetic transition near 440 K and ferroelectric transition near 1050 K.[7] In bulk form hexagonal RFeO$_3$ is metastable thus the sample synthesis is quite difficult. Very recently, it was found that the hexagonal phase of RFeO$_3$ can be stabilized when doped with 50% Sc in $Lu_{1-x}Sc_xFeO_3$.[8] Moreover, $Lu_{0.5}Sc_{0.5}FeO_3$ (LSFO) was reported to exhibit a dielectric anomaly associated with a weak ferromagnetic transition at 162 K, the mechanism of which is not understood at present.

Here, we present evidence from a neutron scattering experiment on a powder sample of $Lu_{0.5}Sc_{0.5}FeO_3$, that two successive antiferromagnetic transitions occur instead, one at $T_{N1} \approx 175$ K and another one at $T_{N2} \approx 70$ K. From inelastic neutron scattering measurements, we observed that the scattering intensity under the magnetic $(100)_M$ reflection change from elastic to inelastic as a function of increasing temperature. The magnetic $(100)_M$ reflection most likely arises from the Γ_1 or Γ_3 magnetic structure, which has the spin orientation arranged in a 120° configuration in the a-b plane. Critical magnetic scattering appears at temperatures well above T_{N1}, and disappears below as the system globally orders. The broad inelastic scattering, which appears in the same region in momentum space as the $(100)_M$ reflection, shows an asymmetric shape below T_{N1} indicating that the magnetic fluctuations are confined in two dimensions. This is consistent with our previous results on LuMnO$_3$.[9]

EXPERIMENT

Polycrystalline LSFO was made using solid-state reaction. Stoichiometric quantities of La_2O_3, Sc_2O_3, and Fe_2O_3 were mixed, ground and pelletized. The pellets were heated in air in Al_2O_3 crucibles at 1000 ℃ for 72 hrs, with three intermediate grindings. The crystal structure and magnetic structures were determined by neutron powder diffraction which were performed using the BT-1 diffractometer at the NIST Center for Neutron Research (NCNR) with a neutron wavelength of λ=2.079 Å. The inelastic data were collected using the Disk-Chopper-Spectrometer (DCS) at NCNR with λ=2.5 Å and 4.5 Å.[10]

DISCUSSION

The neutron powder diffraction pattern of LSFO collected at room temperature is shown in Fig. 1. All the diffraction peaks can be indexed by space group of $P6_3/cm$ as for LMO [9,11] with lattice parameters $a = b = 5.8607(4)$ Å, and $c = 11.7004(3)$ Å. Rietveld refinements were performed to obtain the crystal structural parameters as shown in Table 1. The resulting overall reduced goodness-of-fit parameter, χ^2, is 7.7%. The inset of Fig. 1 shows the lattice structure of LSFO. The FeO_5 bipyramids share the in-plane oxygen ions to form a triangular lattice in the *ab* plane and are separated along the *c* axis by Lu/Sc layers. The cooperative tilting of FeO_5 bipyramids and the buckling of Lu/Sc layers give rise to the ferroelectricity. The magnetic property of LSFO is dominated by the antiferromagnetic (AFM) interaction between the spins of the Fe^{3+} ions on the triangular lattice in the *ab* plane. Since the magnetic Fe^{3+} ions are arranged in the layered triangular lattice, the hexagonal LSFO is expected to be a magnetic frustrated system.

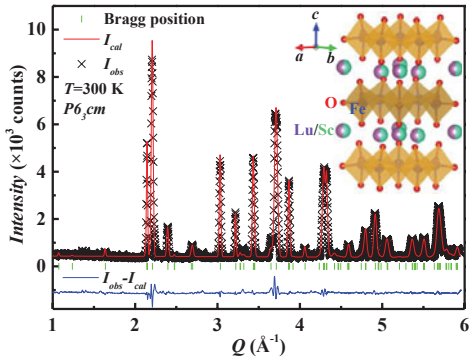

Figure 1. Neutron powder diffraction data (cross) and Rietveld refinement pattern (solid red curve) for LSFO at 300 K with Bragg reflections marked by vertical ticks, and the difference between data and Rietveld model in blue beneath. The insert shows the crystal structure obtained from Rietveld refinement.

Table 1. Refined Structural Parameters of Hexagonal $Lu_{0.5}Sc_{0.5}FeO_3$ at 300 K.

atom	site	*x*	*y*	*z*
Lu_1/Sc_1	2a	0	0	0.54522(0)

Lu_2/Sc_2	4b	1/3	2/3	0.51378(6)
Fe	6c	0.35073(4)	0	0.27740(5)
O_1	6c	0.28738(0)	0	0.43821(6)
O_2	6c	0.66874(0)	0	0.60896(6)
O_3	2a	0	0	0.76593(7)
O_4	4b	1/3	2/3	0.30006(3)

The onset of antiferromagnetic order is determined from neutron diffraction as shown in Fig. 2(a). At 4.5 K we find diffraction peaks corresponding to structurally forbidden $(100)_M$ and $(101)_M$ reflections.[9,11] No noninteger reflections were observed indicating that the magnetic unit cell is the same as the crystalline one. With decreasing temperature the $(101)_M$ reflection appears first at around 175 K corresponding to the AFM Neel transition temperature. The intensity of $(101)_M$ reflection reaches a maximum near 70 K and decreases with further decreasing temperature. Below 70 K, the structurally forbidden $(100)_M$ reflection appears and the intensity rises with further cooling. These results indicate that two successive AFM transitions occur, the AFM one at $T_{N1} = 175$ K and another due to spin-reorientation transition at $T_{N2} \approx 70$ K. The magnetic ground state and spin reorientation in LSFO can be understood from representational analysis. The results are three representations describing different 120° type magnetic structures in each plane.[11] Fig. 2(b) shows the possible magnetic structures below T_{N1} . The ground state can be described entirely by the Γ_1 or Γ_3 type. Since Γ_1 and Γ_3 representations form a homometric pair, they cannot be distinguished using unpolarized neutron scattering. With increasing temperature, spins rotate into a new structure, which can be explained by the Γ_2 model. The Γ_2 structure exists over the temperature range $T_{N1}>T>T_{N2}$.

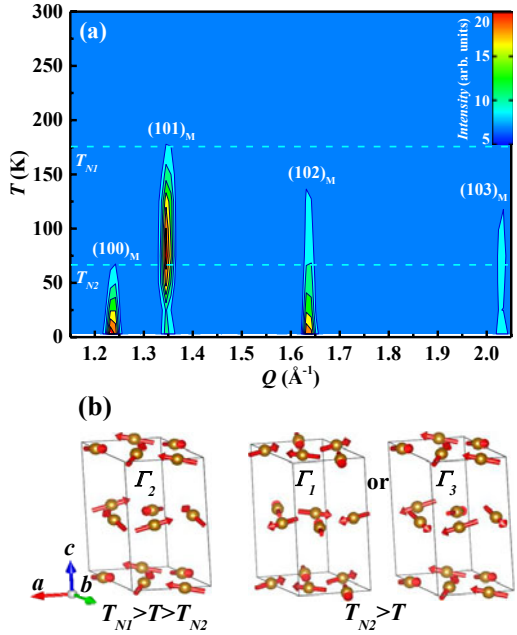

Figure 2. (a) Neutron diffraction intensities for the magnetic reflections as a function of temperature. (b) Magnetic structures obtained from magnetic diffraction analysis.

In order to explore the magnetic dynamics of LSFO, inelastic neutron scattering experiments were performed. The results with an incident neutron wavelength λ = 2.5 Å are illustrated in Fig. 3. In Figs. 3(a)–3(c), the neutron scattering intensity is plotted as a contour map of energy versus momentum transfer, $\hbar\omega$–Q, at three temperatures, 200 K, 100 K, and 1.5 K. A strong inelastic scattering intensity is clearly visible, emanating from $Q \approx 1.25$ Å^{-1} and extending well into the inelastic regime. The scattering exhibits a strong temperature dependence as can be seen from a comparison between the three contour maps. The inelastic scattering intensity appears strong at 200 K, which is well above the AFM ordering temperature T_{N1}. It subsides by 100 K and barely present at 1.5 K. The Q dependence of the inelastic scattering intensity $I(Q)$ was obtained by integrating the intensity along the energy axis with 1 meV < $\hbar\omega$ <10 meV, as shown in Fig. 3(d). A broad peak clearly visible near $Q \approx 1.25$ Å^{-1} corresponds to the $(100)_M$ magnetic reflection. Distinct differences in the inelastic spectra are observed above and below T_{N1}. Below T_{N1}, the overall shape of the integrated intensity is asymmetric while above T_{N1}, it is symmetric. Fig. 3(d) also shows that the inelastic intensity is present all the way down to 1.5 K. The inset of Fig. 3(d) shows the integrated intensity as a function of temperature for the peak near $Q \approx 1.25$ Å^{-1}. The integrated intensity decreases with cooling and shows a drop

at T_{N1}.

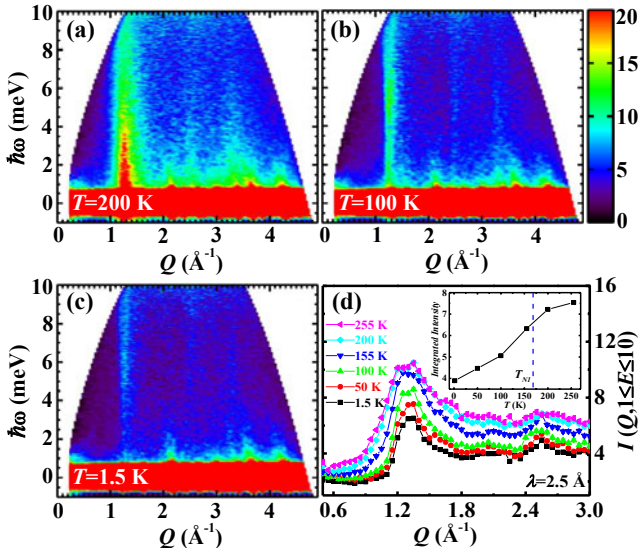

Figure 3. Inelastic neutron scattering contour maps of energy ($\hbar\omega$) versus momentum transfer (Q) at (a) 200 K, (b) 100 K, and (c) 1.5 K with λ=2.5 Å. (d) Q dependence of the energy integrated neutron scattering intensities. The insert shows the Q integrated intensities of the broad peak near $(100)_M$ as as function of temperature.

Using an incident neutron wavelength λ = 4.5 Å, the resolution improves further at $Q \approx 1.25$ Å^{-1}. The results are shown in Fig. 4. Similar to the results of λ = 2.5 Å, the inelastic scattering intensity decrease with decreasing temperature. The Q dependence of the inelastic scattering intensity was obtained by integrating the intensity along energy axis with 0.2 meV < $\hbar\omega$ < 2.5 meV, as shown in Fig. 4(d). The asymmetric characteristics of the $I(Q)$ below T_N is more clear than that of λ = 2.5 Å. Furthermore, the asymmetric characteristics is enhanced by cooling from 155 K to 100 K. At the lowest temperature of 1.5 K, the inelastic intensity is very broad and weak, indicating that the scattering is mainly in the elastic channels. The strong inelastic neutron scattering intensity observed at $Q \approx 1.25$ Å^{-1} correspond to nearest neighbor Fe–Fe spin correlation. Similar features have been observed in geometrically frustrated magnetic materials such as in $CuCrO_2$ and ZnV_2O_4.[12,13] Such asymmetry is indicative of a lower dimensionality, characteristic of the magnetic interactions. The asymmetry in the structure function suggests that the fluctuations are confined in the Fe plane. The fact that the inelastic intensity is present all the way down to 1.5 K indicates that fluctuations persist well below T_{N1}, and that the system remains frustrated even after magnetic ordering sets in.

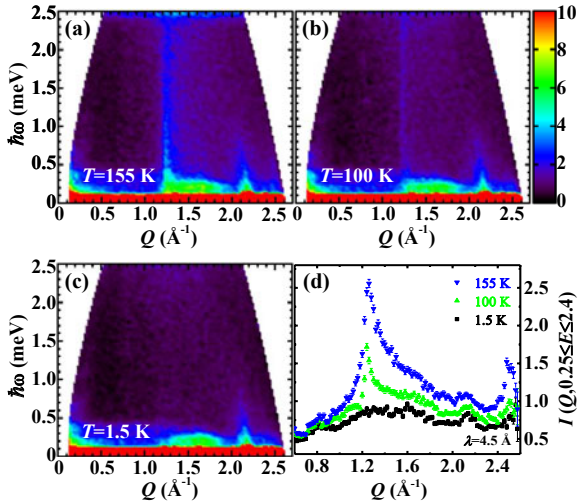

Figure 4. Inelastic neutron scattering contour maps of energy ($\hbar\omega$) versus momentum transfer (Q) at (a) 155 K, (b) 100 K, and (c) 1.5 K with λ = 4.5 Å. (d) Q dependence of the energy integrated neutron scattering intensities.

CONCLUSIONS

To conclude, two successive AFM transitions in LSFO were observed. The scattering intensity under the magnetic $(100)_M$ reflection change from elastic to inelastic as a function of temperature. Critical magnetic scattering appears at temperatures well above T_{NI}, and disappears below as the system globally orders. The broad inelastic scattering, which appears in the same region in momentum space as the $(100)_M$ and $(101)_M$ reflections, shows an asymmetric shape below T_{NI} indicating that the magnetic fluctuations are confined in two dimensions. This is consistent with our previous results on $LuMnO_3$. This seems to be a quite common feature in this class of materials.

ACKNOWLEDGMENTS

We thank Dr. Wei Zhou for assistance in the DCS data collection. This work is supported by the U.S. Department of Energy under contracts DE-FG02-01ER45927 at the University of Virginia. Neutron scattering in this work was performed partly under the Center for High Resolution Neutron Scattering (CHRNS) that is jointly funded by the National Science Foundation under Agreement Number DMR-1508249, and by the NCNR.

REFERENCES

1. T. Kimura, *Annu. Rev. Mater. Res.* **37**, 387 (2007).
2. H. Katsura, N. Nagaosa, and A. V. Balatsky, *Phys. Rev. Lett.* **95**, 057205 (2005).
3. S.-W. Cheong and M. Mostovoy, *Nat. Mater.* **6**, 13 (2007).
4. T.-h. Arima, *J. Phys. Soc. Jpn.* **80**, 052001 (2011).
5. B. B. Van Aken, Thomas T.M. Palstra, Alessio Filippetti and Nicola A. Spaldin, *Nat. Mater.* **3**, 164 (2004).
6. D.-Y. Cho, J.-Y. Kim, B.-G. Park, K.-J. Rho, J.-H. Park, H.-J. Noh, B. J. Kim, S.-J. Oh, H.-M. Park, J.-S. Ahn, H. Ishibashi, S-W. Cheong, J. H. Lee, P. Murugavel, T. W. Noh, A. Tanaka, and T. Jo*, Phys. Rev. Lett.* **98**, 217601 (2007).
7. Wenbin Wang*,* Jun Zhao, Wenbo Wang, Zheng Gai, Nina Balke, Miaofang Chi, Ho Nyung Lee, Wei Tian, Leyi Zhu, Xuemei Cheng, David J. Keavney, Jieyu Yi, Thomas Z. Ward, Paul C. Snijders, Hans M. Christen, Weida Wu, Jian Shen, and Xiaoshan Xu, *Phys. Rev. Lett.* **110**, 237601 (2013).
8. Atsunobu Masuno, Atsushi Ishimoto, Chikako Moriyoshi, Naoaki Hayashi, Hitoshi Kawaji,Yoshihiro Kuroiwa and Hiroyuki Inoue, *Inorg. Chem.* **52**, 11889 (2013).
9. Shin-ichiro, Despina Louca, Songxue Chi, Masaaki Matsuda, Yiming Qiu, John R. D. Copley, and Sang-Wook Cheong, *J. Phys. Soc. Jpn* **83**, 024601 (2014).
10. J.R.D. Copley and J.C. Cook, *Chem. Phys*. 292, 477 (2003).
11. P. Tong, D. Louca, N. Lee, and S.-W. Cheong, *Phys. Rev. B* **86**, 094419 (2012).
12. Steven M. Disseler, Xuan Luo, Bin Gao, Yoon Seok Oh, Rongwei Hu, Yazhong Wang, Dylan Quintana, Alexander Zhang, Qingzhen Huang, June Lau, Rick Paul, Jeffrey W. Lynn, Sang-Wook Cheong, and William Ratcliff II, *Phys. Rev. B* **92**, 054435 (2015).
13. M. Poienar, F. Damay, C. Martin, J. Robert, and S. Petit, *Phys. Rev. B* **81**, 104411 (2010).
14. S.-H. Lee, D. Louca, H. Ueda, S. Park, T. J. Sato, M. Isobe, Y. Ueda, S. Rosenkranz, P. Zschack, J. Íñiguez, Y. Qiu, and R. Osborn, *Phys. Rev. Lett.* **93**, 156407 (2004).